

Advancing Hybrid Quantum Neural Network for Alternative Current Optimal Power Flow

Ze Hu, *Student Member, IEEE*, Ziqing Zhu, *Student Member, IEEE*, Linghua Zhu, *Senior Member, IEEE*, Xiang Wei, Siqi Bu, *Senior Member, IEEE*, Ka Wing Chan, *Member, IEEE*

Abstract—Alternative Current Optimal Power Flow (AC-OPF) is essential for efficient planning and real-time operation in power systems but is NP-hard and non-convex, leading to significant computational challenges. Neural networks (NNs) offer computational speedups in solving OPF but face issues like dependency on large datasets, scalability limitations, and inability to enforce physical constraints, compromising solution reliability. To overcome these limitations, this paper proposes hybrid Quantum Neural Networks (QNNs) that integrate quantum computing principles into neural network architectures. Leveraging quantum mechanics properties such as superposition and entanglement, QNNs can capture complex input-output relationships more effectively and learn from small or noisy datasets. To further improve the performance of QNNs and investigate the interplay between classical and quantum components in hybrid architectures, we incorporate advanced techniques including residual learning and physics-informed machine learning into the hybrid QNN designs. These enhancements aim to boost convergence efficiency, lower errors, superior generalization, and robustness to quantum noise. Simulation results demonstrate that these enhanced hybrid QNNs outperform typical hybrid QNNs in solving OPF problems. This work provides valuable insights into the design and optimization of hybrid QNNs, highlighting the potential of quantum computation for broader applications in power systems.

Index Terms—Optimal power flow, quantum neural network, physical-informed neural network, residual learning

I. INTRODUCTION

A. Background

ALTERNATIVE Current Optimal Power Flow (AC-OPF) is a critical optimization problem integral to the operations and strategic planning of various stakeholders—including system operators and electricity market participants—for the efficient and reliable planning and real-time control in power systems. This pervasive reliance underscores OPF’s centrality in power systems; in the United States alone, OPF influences economic activities exceeding ten billion dollars annually [1], [2].

One of primary objective of OPF is to minimize operational costs while satisfying physical constraints such as line capacities and bus voltages by determining the optimal power generation setpoints. However, the OPF problem is both NP-hard and non-convex, resulting in significant convergence challenges and protracted computational times for most solvers [3]. Furthermore, OPF must be computed repeatedly in many application scenarios, including electricity market clearing and bidding strategy determination, underscoring the necessity for

fast and accurate OPF solutions. To address these challenges and ensure rapid computation with convergence guarantees, a substantial body of literature focuses on deriving approximations of the AC-OPF problem, with the linearized DC-OPF being one of the most prevalent methods [4]. Despite these advancements, AC-OPF remains indispensable for achieving a more accurate representation of power system operations, necessitating further improvements in computational efficiency and convergence speed.

B. Related works

In recent years, there has been a keen interest in employing machine learning methods, particularly neural networks (NNs), to estimate solutions of the AC-OPF problem [5]–[7]. Compared to traditional approaches, NNs demonstrate strong performance in learning non-convex functions and have exhibited computational speedups ranging from 100 to 1,000 times [8]. Moreover, multiple newly developed variants of NN are applied to address traditional challenges in OPF solution like computational burden. For instance, by exploiting the graph nature of the power grid, [9] applied graph neural network (GNN) is used to process node information locally in OPF problems, meriting better scalability. One draw-back of approaches mentioned above in solving AC-OPF is not inherently enforcing network constraints. To address this limitation, physics-informed neural networks (PINNs), which incorporate physical laws as additional loss functions during training, have been introduced to complement standard NNs and avoid security constraint violation [8], [10]. Despite their promising performance in OPF problems, NNs face several challenges in real-world implementation. First, NN performance in solving OPF depends heavily on large, high-quality training datasets, making them vulnerable to common machine learning issues such as data insufficiency or loss in available datasets. Second, training complexity grows rapidly with system size. As input and output dimensionality increases, NNs require more neurons and layers to model the system, which complicates training process and demands substantial computational resources.

At the same time, quantum computing methods are becoming increasingly popular in both academia [11]–[14] and industry [15]–[17]. Most quantum methods can be realized on two main paradigms of quantum computing: adiabatic quantum computation (AQC) and gate-based quantum computation (GQC). The former paradigm, AQC, solves problems by leveraging the adiabatic theorem of quantum mechanics

[18], finding solutions by evolving a simple quantum system into a more complex one with small steps while remaining in the ground state throughout the whole process [19]. On the other hand, GQC, considered the “standard” model of quantum computation [20], stores data in quantum bits (qubits) and operates on them using quantum gates within circuit models. A majority of quantum computation applications in power systems lie in the GQC paradigm [21]–[24], especially since quantum devices first demonstrated computational advantages over classical devices [25]. For example, the Harrow–Hassidim–Lloyd algorithm (HHL) has been applied to solve the DC-OPF problem and achieved superior performance in small-scale systems [21], [22]. Results highlighted the exponential speedup of HHL in solving a system of linear equations (SLE) over classical computers. However, the performance of GQC methods is sensitive to their environment (noisy) and prone to quantum decoherence on the widely used noisy intermediate-scale quantum (NISQ) devices [26]. For their robustness to noise, parametrized quantum circuit (PQC), which has tunable parameters in the quantum gates and is optimized by a classical outer loop to solve a specific task, becomes a competitive method and applied in many practical scenarios [25]. In [23], a high expressibility, low-depth (HELD) quantum circuit has been designed and trained by a quantum natural gradient to solve the transient stability assessment in the bulk power systems.

By incorporating PQC as layers within neural networks, quantum neural networks (QNNs) represent a new class of machine learning models that enhance classical methods by leveraging quantum effects such as superposition, entanglement, and interference [27]. Notably, it has been demonstrated in [28] that QNNs can generalize effectively from very small datasets and exhibit remarkable tolerance to noisy training data. Furthermore, QNNs offer the ability to explore high-dimensional feature spaces by utilizing the tensor product structure of Hilbert spaces, thereby opening up possibilities for superior performance in practical applications [29]. These advantages of QNN mentioned above make it a strong candidate for non-convex power systems applications like power flow analysis and AC-OPF [30]. For instance, works in [24] adopted a hybrid QNN in power flow analysis by integrating PQCs with multilayer perceptrons (MLPs), demonstrating a better generalization performance across network topology and robustness to noisy data.

C. Contributions and paper organization

Despite significant advancements in QNN applications, there remain critical gaps in systematic exploration and understanding. 1) Although some early attempts have initiated the application of QNNs to power system tasks, such as power flow analysis [24], and laid the groundwork for further research, the application of QNNs to solve OPF problems remains unexplored. Moreover, the design and optimization of QNNs for enhanced performance in AC-OPF tasks is still an open question. 2) Meanwhile, key challenges associated with QNNs, such as their sensitivity to quantum noise, have yet to be fully addressed. Overcoming these issues is essential to improving their robustness and ensuring reliable

performance in practical applications. 3) The relationship and trade-offs between classical and quantum components in hybrid QNNs remain insufficiently explored. At the start of the century, it was recognized that not all components of a QNN architecture need to be quantum for quantum advantages to emerge [31]. Several studies [31], [32] have demonstrated that a fully quantum neural network may not always outperform hybrid quantum-classical networks, and in some cases, may yield inferior results. Integrating classical (non-quantum) and quantum components in QNNs has been shown to enhance their representational capabilities compared to purely classical or purely quantum networks. Therefore, a more detailed investigation into the integration of classical and quantum components in hybrid QNNs presents an open yet promising research direction, particularly in terms of improving estimation performance.

In light of these gaps, this paper aims to investigate the interplay between classic and quantum components in hybrid QNNs, using the NP-hard AC-OPF problem as a practical case study. On the one hand, the QNNs can be well-trained to solve specific problems with even low-quality datasets, reducing reliance on high-quality training sets. On the other hand, the performance of QNN can be further boosted by the most advanced tricks of deep learning. With the recent surge in neural network development, numerous sophisticated variants and advanced techniques have been introduced for wide applications, including residual learning (ResNet), designed for automatic feature extraction, and physics-informed machine learning, which embeds physical laws into the network architecture to solve complex scientific problems. Given the significant impact of these innovations, it is both intuitive and promising to investigate how such advanced techniques can be adapted to enhance hybrid QNN design, potentially driving the broader practical adoption of quantum technologies. As a result, this paper proposed two variants of Hybrid QNN advanced by residual learning (ResNet) and physics-informed machine learning to enhance representation and estimation performance, which takes AC-OPF as a test example on classic systems.

The contributions of this paper are as follows:

- 1) Development of Enhanced Hybrid Quantum Neural Networks: Two novel hybrid QNN architectures are proposed, incorporating residual learning and physics-informed machine learning to improve the design of the non-quantum components in QNNs. Using the AC-OPF problem as a case study, the proposed QNNs demonstrate faster training and lower test errors in estimating both generation set-points and bus voltages compared to conventional QNNs and standard NNs.
- 2) Superior Generalization and Robustness to Quantum Noise: The proposed hybrid QNNs are evaluated across various test systems, consistently exhibiting superior generalization performance. Furthermore, the methods show remarkable robustness to quantum noise, a critical advantage in the current noisy intermediate-scale quantum era, enhancing their practical viability.

The rest of the paper is constructed as follows: The formu-

lation of the AC-OPF problem along with its Karush-Kuhn-Tucker (KKT) conditions are presented in Section II. The fundamentals of quantum computing and novel designs of quantum neural networks are introduced in Section III. The numerical results comparing the proposed approach with benchmark neural networks are shown in Section IV, highlighting the generation performance and robustness to the quantum noise. The paper is concluded in Section V, summarizing the key findings and suggesting directions for future research.

II. PROBLEM FORMULATION

The AC-OPF problem is an optimization problem for ISO to schedule and dispatch resources in both day-ahead and real-time stages. According to the operation requirements, the objective of AC-OPF may be multiple, including generation cost minimization, line loss minimization, etc. The paper uses the typical objective of minimizing the total cost of active power generation. The AC-OPF problem model in compact form is presented as (1).

$$\min_{\mathbf{V}, \mathbf{G}} \mathbf{c}^T \mathbf{G} \quad (1a)$$

$$\text{s.t. } \mathbf{V}^T \mathbf{L}_l \mathbf{V} = \mathbf{a}_l^T \mathbf{G} + \mathbf{b}_l^T \mathbf{D}, \quad l = \{1, 2, \dots, N_L\} : \rho_l \quad (1b)$$

$$\mathbf{V}^T \mathbf{M}_m \mathbf{V} \leq \mathbf{d}_m^T \mathbf{D} + \mathbf{f}_m, \quad m = \{1, 2, \dots, N_M\} : \mu_m \quad (1c)$$

In the optimization problem above, \mathbf{c}^T is the combined linear cost terms for the active and reactive power generations, $\mathbf{G} = [\mathbf{P}_g^T, \mathbf{Q}_g^T]^T$, $\mathbf{D} = [\mathbf{P}_d^T, \mathbf{Q}_d^T]^T$. Voltage vector $\mathbf{V} = [(\mathbf{V}^r)^T, (\mathbf{V}^i)^T]^T$ contains both the real and imagination part of voltage at all buses. \mathbf{L} and \mathbf{M} are combined vectors that stand for expressions of multiple constraints, please refer to [8] for details. \mathbf{a}_l and \mathbf{b}_l are vectors mapping generation and demands to the corresponding buses. \mathbf{d}_m is the vector mapping active and reactive power of demand in \mathbf{D} to corresponding constraints. \mathbf{f}_m stands for vectors of bounded values for voltage and line flows. ρ_l and μ_m are dual variables for constraints (1b) and (1c), respectively. N_L is the number of constraints in (1b), which is equal to 2 times number of bus N_b plus 1. N_M is the number of constraints in (1c), which is equal to 4 times number of generators N_g plus 2 times N_b plus number of lines N_l .

In the proposed model, the objective in (1a) is to minimize the cost of power generation, subject to compact form constraints of (1b) and (1c). Constraint (1b) denotes all equality constraints, including $2N_b$ constraints for bus power injection and 1 constraints for angle reference of the slack bus. (1c) stands for all inequality constraints, including $4N_g$ constraints for optimal power generation, $2N_b$ constraints for bus voltage, and N_l constraints for line current flow. Based on the optimization above, the Lagrangian function for the AC-OPF can be formulated as (2).

$$\mathcal{L}(\mathbf{x}, \rho, \mu, \mathbf{D}) = \mathbf{c}^T \mathbf{G} + \sum_{l=1}^L \rho_l (\mathbf{V}^T \mathbf{L}_l \mathbf{V} - \mathbf{a}_l^T \mathbf{G} - \mathbf{b}_l^T \mathbf{D}) + \sum_{m=1}^M \mu_m (\mathbf{V}^T \mathbf{M}_m \mathbf{V} - \mathbf{d}_m^T \mathbf{D} - \mathbf{f}_m) \quad (2)$$

Given the optimization problem and its Lagrangian function, the KKT conditions for the AC-OPF are presented in (1b)-(1c) and (3)-(6), where the stationarity condition is given in (3) and (4), the complementary slackness condition is given by (5), and dual feasibility is given by (6).

$$\mathbf{c} = \sum_{l=1}^L \rho_l \mathbf{a}_l \quad (3)$$

$$\left(\sum_{l=1}^L \rho_l \mathbf{L}_l + \sum_{m=1}^M \mu_m \mathbf{M}_m \right) = 0 \quad (4)$$

$$\mu_m (\mathbf{V}^T \mathbf{M}_m \mathbf{V} - \mathbf{d}_m^T \mathbf{D} - \mathbf{f}_m) = 0, \quad m = \{1, 2, \dots, M\} \quad (5)$$

$$\mu_m \geq 0, \quad m = \{1, 2, \dots, M\} \quad (6)$$

(1b) – (1c)

In practical scenarios, grid operators often need to address stochastic AC-OPF problems multiple times within a specified time window. However, the inherent NP-hard and nonconvex nature of the AC-OPF problem poses significant computational challenges. No existing solver can guarantee an exact solution for general AC-OPF problems within polynomial time unless P = NP. This challenge has driven research efforts aimed at reducing the computational time required to solve AC-OPF problems.

III. DESIGN OF HYBRID QUANTUM NEURAL NETWORK FOR AC-OPF

This section introduces the fundamentals of QNN and the typical design of hybrid QNNs. Residual connection (ResNet) and physics-informed layer are then employed to design different types of hybrid QNN to enhance its performance in solving OPF.

A. Fundamentals of Quantum Neural Networks

A qubit, fundamentally defined by complex probability amplitudes, can be represented on the Bloch sphere using two angular coordinates. The schematic representation of a qubit is shown in Fig. 1. Unlike a classical bit that resides definitively in either state 0 or 1, a qubit inhabits a quantum superposition of both states until it is measured. This means the qubit's state is a linear combination of the basis states $|0\rangle$ and $|1\rangle$, introducing inherent probabilistic behavior. This probabilistic nature enhances the ability of QNNs to generalize from data and increases their robustness to noise.

QNNs are built as parameterized quantum circuits (PQC) within the continuous-variable (CV) framework, where quantum information is encoded in continuous parameters like the amplitudes of electromagnetic fields. Much like classical neural networks, QNNs are trained using classical optimization algorithms to learn the mapping between input features \vec{x} and output labels \vec{y} . As depicted in Fig.2, a QNN constitute feature mapping, an ansatz, and a measurement.

Within the PQC, two primary types of quantum gates are employed: 1) the rotation operator gate R and 2) the controlled NOT (CNOT) gate. The rotation operator gates, $X(\theta)$

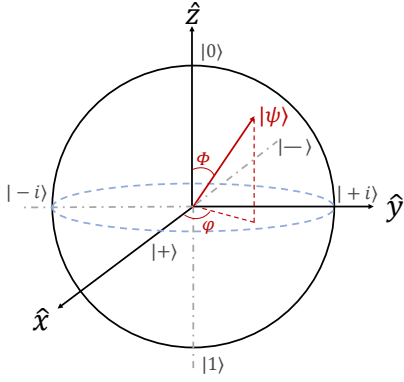


Fig. 1: Illustration of a qubit

and $R_y(\theta)$, represent rotation matrices along two Cartesian axes, where θ denotes the rotation angle. These matrices are defined in equations (7) and (8), illustrating rotations along the corresponding axes. The angle θ specifies the extent of rotation applied along each axis.

$$X(\theta) = \begin{bmatrix} \cos(\theta/2) & -i \sin(\theta/2) \\ -i \sin(\theta/2) & \cos(\theta/2) \end{bmatrix} \quad (7)$$

$$R_y(\theta) = \begin{bmatrix} \cos(\theta/2) & -\sin(\theta/2) \\ \sin(\theta/2) & \cos(\theta/2) \end{bmatrix} \quad (8)$$

The connection lines in the ansatz correspond to CNOT gates, which act on two qubits. The CNOT gate performs a NOT operation on the second qubit only when the first qubit is in the state $|1\rangle$. The training process begins with the feature mapping, where the input data \vec{x} is encoded into the quantum states of multiple qubits. Notably, the selection of the feature mapping strategy is crucial for the QNN's performance, yet it typically remains fixed and is not adjusted during training. After encoding, QNN applies sequences of quantum gates with tunable parameters to form an ansatz—a trial solution that the network adjusts to minimize the loss function. Following the quantum computations, measurements are taken from the qubits. These measurements are then processed classically to generate predictions or labels, which are evaluated against the actual outputs using a loss function.

Specifically, the optimization of the QNN involves adjusting the parameters within the PQCs to minimize the loss function. This is typically achieved using gradient-based optimization methods. Efficient calculation of gradients in QNNs is made possible by analytical techniques for computing the derivatives of expectation values of quantum observables with respect to circuit parameters. These techniques enable the effective training of QNNs despite the complexities introduced by quantum computations. The representation of QNNs can be expressed as follows.

$$|\psi^{\text{in}}\rangle = U(\vec{x})|0 \dots 0\rangle, \quad (9a)$$

$$|\psi^{\text{out}}\rangle = \omega(\vec{w}^r)|\psi^{\text{in}}\rangle \quad (9b)$$

The input state $|\psi^{\text{in}}\rangle$ is generated by transforming $\vec{x} \in \{\bar{p}_i, \bar{q}_i : i = 1, 2, \dots, n\}$ into valid quantum states using the

feature map $U(\cdot)$, which is applied to the vacuum state $|0 \dots 0\rangle$. The ansatz $\omega(\cdot)$ is then applied to $|\psi^{\text{in}}\rangle$. Notably, the feature map does not involve any parameters that require optimization. In contrast, the vector of adjustable parameters for the ansatz, denoted by \vec{w}^r , is fine-tuned during the training process using a dataset comprising N training pairs \vec{x}, \vec{y} . The resulting output state $|\psi^{\text{out}}\rangle$ cannot be directly observed; instead, it must be inferred through measurement, yielding $\hat{y} \in \{\vec{v}_i, \vec{\delta}_i\} : i = 1, 2, \dots, n$.

B. Hybrid Quantum Neural Networks

With the fundamentals of typical QNN, we implement hybrid QNNs that integrate a pure QNN as an intermediate layer within a traditional neural network framework into the AC-OPF problem. The brief structure of Hybrid QNN is depicted in Fig. 2. Data flow initiates from the input layer and the first hidden layer of the NN, traverses through the feature map and ansatz within the PQC, and, following measurement, proceeds to subsequent classical hidden layers and output layer. Afterward the final layer, the active and reactive power generation are output as the solution results. Notably, hybrid QNNs emulate an autoencoder in the proposed structure, where the initial classical component encodes the input x into a lower-dimensional latent space on which the QNN operates. Subsequently, the second classical component deciphers the measurement outcomes back into a higher-dimensional space to produce the output. This architecture inherently offers the flexibility to accommodate larger input features and output labels pertinent to large-scale power systems, as it is not constrained by the limited number of available qubits.

To train the Hybrid QNN with back-propagation to improve the solution accuracy for the AC-OPF, the loss function L_{nn} is represented by (10), containing Mean Absolute Error (MAE) of active and reactive power generation G , bus voltage and angle v , and Lagrangian multipliers L . Λ are predefined parameters to weight terms. N_t is the number of training instance.

$$L_{\text{nn}} = \frac{1}{N_t} \sum_{i=1}^{N_t} (\Lambda_P \frac{|\hat{G} - G|}{\text{MAE}_g} + \Lambda_V \frac{|\hat{v} - v|}{\text{MAE}_v} + \Lambda_L \frac{|\hat{L}_m - L_m|}{\text{MAE}_l}) \quad (10)$$

C. Residual Learning (ResNet)

Residual learning, which leverages shortcut connections between layers in neural networks (NNs), was initially introduced for image recognition tasks [33]. By mitigating vanishing and exploding gradient problems, residual learning substantially enhances the performance of NNs across diverse tasks; moreover, the benefits amplify with increased network depth. Drawing inspiration from [33], [34], we propose two variants of residual-connected hybrid QNNs. The first variant incorporates shortcut connections between every two layers. In contrast, the second variant conceptualizes the hybrid QNN as an encoder-decoder architecture, with the NN components before and after the parameterized quantum circuit (PQC) serving as the encoder and decoder, respectively. In this

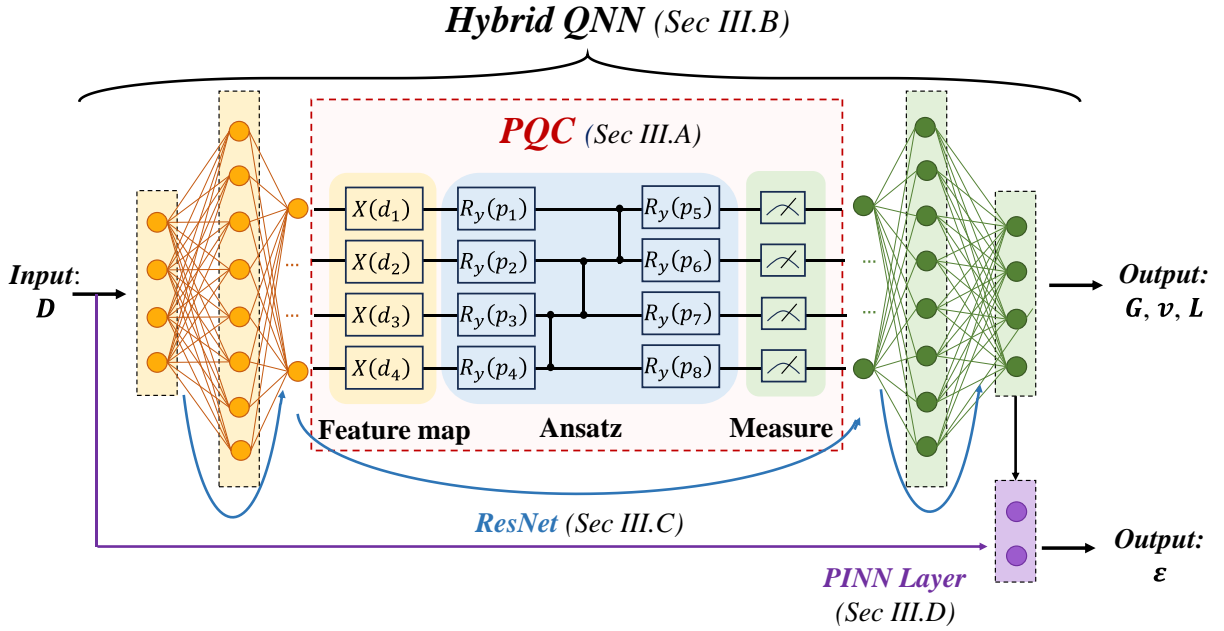


Fig. 2: Structure of a Hybrid QNN using residual connection and physics-informed layer

configuration, shortcut connections are established as identity mappings from each encoding layer to its corresponding mirrored decoding layer in a nested manner.

1) *Sequential Residual Connection*: Sequential connections enable typical residual shortcuts from the input of the first layer to the output of the second layer before the activation function [33]. The detailed implementation is shown in Fig. 3a. This is one of the most commonly used methods for constructing residual connections and assumes that the whole NN gradually processes different features of the input. It can be represented by (11).

$$y_l = x_l + f_l(x_l, W_l) \quad (11)$$

In (11), x_l and y_l are the input and output for layer l , respectively. W_l denotes the parameters for the layer l . In addition, the layer output y_l is input to a activation function, e.g., rectified linear unit (ReLU), for non-linear transformation and then be the input of the next layer, which is shown in (12).

$$x_{l+1} = \text{Relu}(y_l) \quad (12)$$

2) *Nested Residual Connection*: The "nested" residual connections indicate the residual connection from the encoder to its corresponding "mirror" layer in the decoder. This kind of connection implies an assumption that these mirror layers encode or decode the same level of features in the NN. The implementation is presented in Fig. 3b. Assuming the PQC as the latent layer Q , the encoder layer 1, and its mirror decoder layer L . With the residual identity connection, it can be presented as

$$y_L = x_l + f_L(x_L, W_L) \quad (13)$$

where x_l and y_l denote the input and output of the l layer, x_L and y_L are the input and output of the L layer. The W_l and

W_L indicate parameters for the corresponding l and L layers. $f_L()$ is the layer function including activation. As the decoder layer is behind the encoder and also the latent layer, equation (13) can be reformulated by (14), where $q_L(f_L(x_l, W_l), W_q)$ stands for the function of encoder input x_l for decoder output x_L , indicating multi-layer transformation.

$$y_L = x_l + f_L(q_L(f_L(x_l, W_l), W_q), W_L) \quad (14)$$

From automatic differentiation [34], the general derivative of the loss function for x_l can be used to compute the gradients for the parameters of the previous layer as (15), where the activation function and batch normalization are omitted for simplicity but are added to improve representation ability and avoid the "vanishing gradient" problem in implementation.

$$\frac{\partial L_{nn}}{\partial x_l} = \frac{\partial L_{nn}}{\partial y_L} \cdot \left(1 + \frac{\partial}{\partial x_l} (f_L(g_L(f_l(x_l, W_l)), W_L)) \right) \quad (15)$$

The constant 1 in the loss function above directly propagates the information from the decoder layer to the corresponding encoder layer. Also, the second term after the constant 1 is not always -1 , which may cancel out the gradient. Therefore, gradient vanishing and subsequent degradation of performance can be partially avoided during backward propagation. Such shortcuts can also improve the training speed due to the direct pass of the gradient.

D. Physics-informed Neural Network

PINNs are a class of neural networks trained to solve supervised learning tasks while adhering to physical laws described by nonlinear equations [35]. Specifically, PINNs integrate an additional physics layer after the typical neural network output to estimate the differential terms of the output variables. This integration allows the discrepancies in these

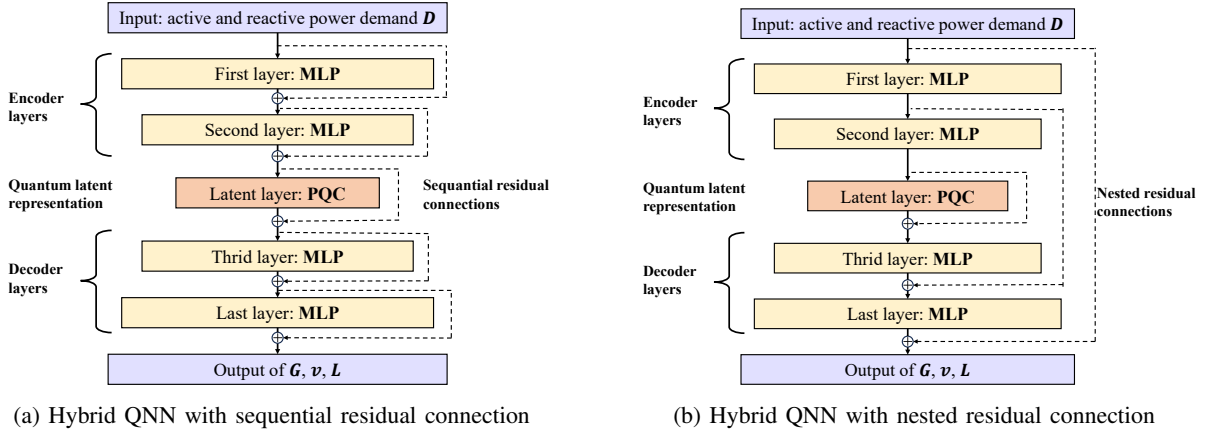


Fig. 3: Structure of Hybrid QNN with two types of residual connections

differential terms—representing the “physical loss”—to be incorporated into the neural network’s training loss function, calculated using the error between the estimated and actual differential variables. Consequently, the neural network’s output solution is validated against the loss associated with the physical constraints.

In the context of the AC-OPF problem, the PINN architecture aims to predict the active and reactive power generation setpoints G , with the active and reactive power demands D serving as inputs. The structure of the PINN under AC-OPF is presented as Fig.4. Since the optimal solution must satisfy the KKT conditions specified in (1b)-(1c) and (3)-(6), the discrepancies in the KKT conditions—as shown in (16-a) to (16-d)—represent the physical loss and assist in the neural network’s training as outlined in equation (10).

$$\epsilon_{\text{stat}} = \left| c - \sum \hat{\rho}_l a_l \right| + \left| \left(\sum \hat{\rho}_l L_l + \sum \hat{\mu}_m M_m \right) \right| \quad (16\text{-a})$$

$$\epsilon_{\text{comp}} = \sum \left| \hat{\mu}_m \left(\hat{V}^T M_m \hat{V} - d_m^T D - f_m \right) \right| \quad (16\text{-b})$$

$$\epsilon_{\text{dual}} = \pi(\hat{\mu}_m) \quad (16\text{-c})$$

$$\epsilon_{\text{prim}} = \sum \left| \hat{V}^T L_l \hat{V} - a_l^T G - b_l^T D \right| \quad (16\text{-d})$$

By combining the mean absolute errors (MAEs) for G , v and L , as well the discrepancy in KKT conditions, the MAE in (17) is used to be the loss function and update the network, where N_c represents the number of collection instant.

$$MAE = \frac{1}{N_t} \sum_{i=1}^{N_t} (\Lambda_P \underbrace{|\hat{\mathbf{G}} - \mathbf{G}|}_{MAE_g} + \Lambda_V \underbrace{|\hat{\mathbf{V}} - \mathbf{V}|}_{MAE_v} + \Lambda_L \underbrace{|\hat{\mathbf{L}}_m - \mathbf{L}_m|}_{MAE_l}) + \frac{\Lambda_\epsilon}{N_t + N_c} \sum_{i=1}^{N_t + N_c} \underbrace{\epsilon_{\text{stat}} + \epsilon_{\text{comp}} + \epsilon_{\text{dual}} + \epsilon_{\text{prim}}}_{MAE_\epsilon} \quad (17)$$

These error terms are weighted by predefined parameters. A significant challenge in training PINNs is the sharp fluctuations that occur during the minimization of the equation loss and boundary-condition losses. Discrepancies in the KKT conditions can lead to suboptimal training performance. To enhance the efficiency of PINNs, various methods—including ensemble learning [36], point-weighting (PW) methods, and

others—have been proposed to expedite the minimization process when dealing with competing error terms. However, since this paper focuses on integrating QNN techniques into PINNs, the weighting parameters in our proposed model are selected arbitrarily.

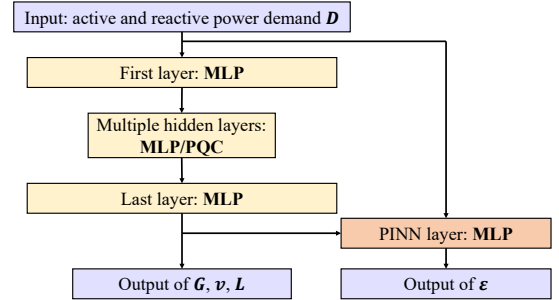


Fig. 4: Detailed illustration of a Hybrid Quantum PINN

Furthermore, collocation points are incorporated into the training set to train the PINN layer by leveraging the KKT conditions to assess the accuracy of the neural network’s predictions. Specifically, collocation points are a set of random input values from the input domain, akin to the NN training data points. However, only the error terms specified in equations (11) are utilized to measure prediction accuracy and train the NN; the optimal generation dispatch values, voltage setpoints, and dual variables are not computed for the collocation points prior to training, and their corresponding errors are set to zero. This technique has been validated to enhance the training efficiency of PINNs [8]. Notably, unlike approaches that employ three independent NNs to compute G , v , and L separately, our PINN model utilizes a single NN to estimate all three types of variables. This unified approach facilitates a more straightforward implementation of QNN techniques, as discussed in the next section.

IV. NUMERICAL RESULTS

A. Simulation setup

The proposed method is evaluated against a standard NN and PINN across several test systems. The details of the net-

work for the 14-bus case are derived from [37]. Additionally, the active and reactive power demands are assumed to be independent of each other.

Ten thousand sets of random active and reactive power input values were generated using Latin hypercube sampling [38]. Among these, 50% were allocated to the collocation data set, for which OPF set-points were not required. Of the remaining data, 20% was used for training, while 30% served as the test data set. AC-OPF in MATPOWER was utilized to determine the optimal active and reactive power generation values and voltage setpoints for the input data points in the training and test sets. The comparison methods include: a typical NN (denoted as M1), PINN (M2), QNN (M3), PIQNN with sequential residual connection (M4), and PIQNN with nested residual connection (M5).

We used Pytorch [39] with Python for classic neural network training and Qiskit [40] for implementation and training process of PQC. To achieve a better performance by using NN, the input of NN, including active and reactive power demand, is normalized to have a mean of 0 and standard deviation of 1. The number of training epochs is fixed to be 1,000 and the data set is split into 50 batches while training. The network training are carried on a PC with Intel(R) Xeon(R) Gold 6230R CPU@ 2.10GHz 2.10 GHz, and 256 GB RAM, and NVIDIA RTX A4900.

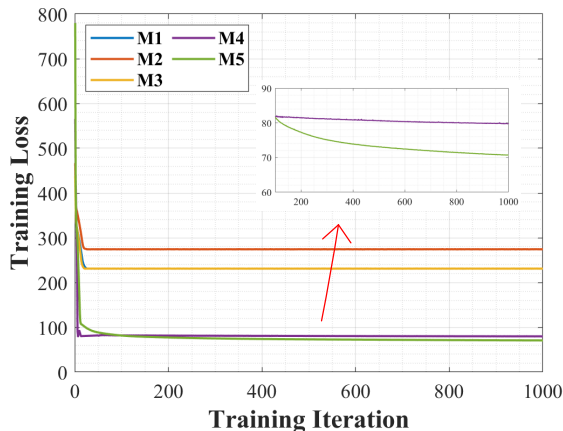


Fig. 5: Training loss curves for comparable methods on the IEEE 39-bus system

B. Network convergence in training set

To evaluate network convergence during training, we present the loss curves for all comparable methods on the IEEE 39-bus system in Fig. 5. At the outset, the loss values for all methods are initially high but rapidly decrease within the first few iterations. After this initial phase, each method follows a distinct trajectory until convergence. Among them, M4 and M5 converge to nearly identical, lowest-loss values, reflecting their superior performance. Interestingly, M4 exhibits an abrupt drop early in training and achieves a very low loss—an observation whose underlying cause is not fully understood. Although M4 and M5 both exhibit relatively low losses, M5 stabilizes at a similarly low level following the initial stage.

Meanwhile, QNN (M3) and NN (M1) display almost identical curves, with losses higher than those of the residual-based methods (M4 and M5) but lower than PINN (M2). Notably, PINN (M2) consistently yields the highest loss throughout the entire training process, likely because of the additional KKT loss term compared to standard neural-network approaches.

C. Validation Under Varying topologies

This subsection evaluates the effectiveness of the proposed method (M1–M5) under varying test systems. Specifically, we compare these methods in the IEEE 14-bus, 39-bus, and 162-bus systems. The performance indicators include the MAE of generator set-points for active and reactive power, as well as bus voltage magnitude and angle. Notably, M4 and M5 are the proposed methods, each employing a different type of residual connection.

From Table I, it is evident that M1–M3 achieve broadly similar results across all three systems. This finding suggests that directly incorporating PQC and a physics-informed layer into a typical NN does not significantly alter its performance in solving AC-OPF.

In contrast, M4 and M5 exhibit the lowest MAEs for nearly all metrics across all test systems. In the IEEE 14-bus system, M5 performs particularly well, reducing MAEs by approximately 60% and 80% for active and reactive power set-points, respectively, and by about 40% and 70% for bus voltage magnitude and angle. Likewise, in the IEEE 39-bus system, M5 achieves around 70% and 50% lower MAEs in active and reactive power set-points, while lowering bus voltage magnitude and angle MAEs by roughly 60% and 80%, respectively. For the IEEE 162-bus system, M4 yields the lowest MAEs for generator set-points—showing about a 40% and 14% improvement—whereas M5 delivers the lowest MAEs for voltage magnitude and angle, also with improvements of about 40% and 14%, respectively.

Focusing on the proposed methods (M4 and M5), their relative performance varies with system size. For instance, M4’s MAEs are comparable to those of M1–M3 in the IEEE 14-bus system and slightly better in the IEEE 39-bus system, although still inferior to M5’s performance. Notably, M4 attains the lowest generator set-point errors in the IEEE 162-bus system, whereas M5’s performance in that larger system is on par with or sometimes worse than M1–M3. These observations indicate that different implementations of residual connections can substantially affect solution accuracy, underscoring the importance of choosing an appropriate residual design for a given system scale.

D. Impact of the Physics-Informed Layer

In this subsection, we evaluate how the physics-informed layer affects model performance by examining how the MAE varies under different values of Λ_ϵ , which represents the weight of the physics loss MAE_ϵ . Table II summarizes the results of the MAE comparison for Λ_ϵ values ranging from 10^{-7} to 10^{-3} . These values are chosen based on the magnitude of both the physics loss and the typical neural-network loss.

TABLE I: MAEs comparison across different test systems

Systems	Models	MAE(P)	MAE(Q)	MAE(V)	MAE(θ)
IEEE 14-bus	M1	0.006175	0.011178	0.001236	0.007191
	M2	0.006180	0.011108	0.001256	0.007213
	M3	0.006289	0.011401	0.002117	0.007303
	M4	0.006281	0.011115	0.001332	0.007177
	M5	0.002254	0.001950	0.000764	0.002057
IEEE 39-bus	M1	0.471165	0.104933	0.005931	0.040568
	M2	0.471104	0.104936	0.005898	0.040596
	M3	0.470773	0.104762	0.005973	0.040089
	M4	0.282898	0.072738	0.004819	0.013834
	M5	0.135084	0.049726	0.002468	0.009207
IEEE 162-bus	M1	34.023755	15.620439	0.027568	1.057711
	M2	34.024110	15.619855	0.028161	1.056532
	M3	34.025294	15.621361	0.026640	1.059286
	M4	20.016157	13.426665	0.148620	0.651906
	M5	38.144987	15.257035	0.100408	0.621210

TABLE II: MAEs comparison for proposed methods with changing physics-informed parameters

Λ_ϵ		1e-7	1e-6	1e-5	1e-4	1e-3
M4	MAE(P)	0.282944	0.282898	0.283021	0.283038	0.283009
	MAE(Q)	0.072753	0.072738	0.072849	0.072630	0.07272
	MAE(V)	0.004848	0.004819	0.004828	0.004838	0.004949
	MAE(θ)	0.013934	0.013834	0.014029	0.013883	0.023536
M5	MAE(P)	0.134472	0.135084	0.151607	0.151567	0.151596
	MAE(Q)	0.049480	0.049726	0.052071	0.052046	0.052085
	MAE(V)	0.002485	0.002468	0.002493	0.002530	0.002461
	MAE(θ)	0.009096	0.009207	0.010785	0.011042	0.020687

From Table II, we observe that the optimal physics-loss weight for M4 is approximately 10^{-6} , yielding the lowest MAEs in active-power set-points and voltage estimation. This finding implies that the physics-informed layer meaningfully enhances M4, as the optimal Λ_ϵ does not tend toward zero. However, selecting a single “best” weight is difficult because the lowest MAEs for different output variables occur at different Λ_ϵ values. In contrast, the performance of M5 improves as Λ_ϵ decreases, suggesting that the physics-informed layer has a greater impact on M4 than on M5.

E. Sensitivity Analysis on Quantum Noise

The sensitivity of typical Hybrid QNN (M3) and proposed novel QNN methods (M4 and M5) on quantum noise is analyzed in this subsection by testing these methods on IEEE 39-bus system with a changing quantum noise. The results are presented in Fig. 6, where the x-axis is the quantum noise level ranging from 0.1 to 0.5, while the y-axis (MAE ratio) is the sum of all MAEs under certain quantum noise divided by the sum MAE without noise. The results indicate that as noise increases, the MAEs of the typical Hybrid QNN (M3) rise significantly. Specifically, the MAE with quantum noise from 0.1 to 0.4 increases about quadratic, while the MAE increasing tendency with the noise level range from 0.3 to 0.5 is about to be linear. This observation highlights the susceptibility of typical QNN to quantum noise. In contrast, the proposed meth-

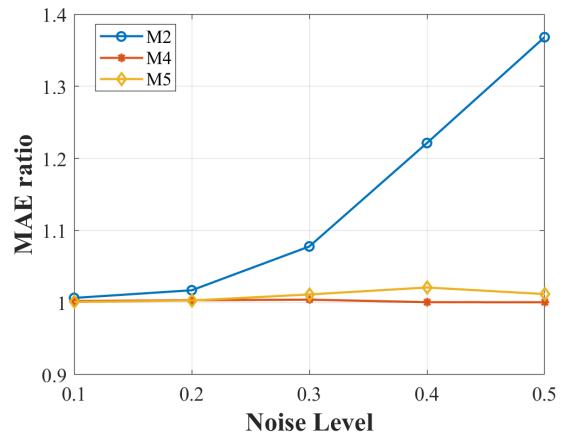


Fig. 6: Illustration of the impact of various noise levels on the performance different QNNs on IEEE 39-bus system

ods M4 and M5 exhibit minimal sensitivity to quantum noise, with negligible increases in MAEs compared to the typical Hybrid QNN. This observation underscores the robustness of the proposed methods against quantum noise, which is a highly desirable property in the noisy intermediate-scale quantum era.

V. CONCLUSION

This paper developed two enhanced hybrid QNN architectures to solve the NP-hard AC-OPF problem by advancing the typical QNNs with residual learning and physical-informed layers. The proposed methods are verified on several classic test systems. Simulation results demonstrates a faster convergence and significant lower errors of the proposed methods compared to typical NNs and hybrid QNNs in AC-OPF problem. The generalized performance to multiple network topologies are also verified. Moreover, the sensitivity analysis indicates that the proposed methods merits the robustness in quantum noise, which is a very favorable property for quantum methods running on noisy intermediate-scale quantum devices. Overall, this paper proposes two potential solutions to AC-OPF problems, validates the usefulness of classic component design in QNN application, and highlights the techniques including residual learning and physics-informed machine learning in QNN design. Potential directions include exploring optimization algorithms for alternative quantum circuit training and extending the approach to larger and more complex power systems.

REFERENCES

- [1] M. B. Cain, R. P. O’neill, A. Castillo *et al.*, “History of optimal power flow and formulations,” *Federal Energy Regulatory Commission*, vol. 1, pp. 1–36, 2012.
- [2] H.-D. Chiang, Z.-Y. Wang, and L. Zeng, “Dynamic relationship between kkt saddle solutions and optimal solutions in ac opf problems,” *IEEE Transactions on Power Systems*, vol. 39, no. 1, pp. 1637–1646, 2023.
- [3] D. Bienstock and A. Verma, “Strong np-hardness of ac power flows feasibility,” *Operations Research Letters*, vol. 47, no. 6, pp. 494–501, 2019.
- [4] P. Kundur, “Power system stability,” *Power system stability and control*, vol. 10, pp. 7–1, 2007.
- [5] L. Duchesne, E. Karangelos, and L. Wehenkel, “Recent developments in machine learning for energy systems reliability management,” *Proceedings of the IEEE*, vol. 108, no. 9, pp. 1656–1676, 2020.

- [6] M. K. Singh, V. Kekatos, and G. B. Giannakis, "Learning to solve the ac-opf using sensitivity-informed deep neural networks," *IEEE Transactions on Power Systems*, vol. 37, no. 4, pp. 2833–2846, 2021.
- [7] M. Zhou, M. Chen, and S. H. Low, "Deepopf-ft: One deep neural network for multiple ac-opf problems with flexible topology," *IEEE Transactions on Power Systems*, vol. 38, no. 1, pp. 964–967, 2022.
- [8] R. Nellikath and S. Chatzivasileiadis, "Physics-informed neural networks for ac optimal power flow," *Electric Power Systems Research*, vol. 212, p. 108412, 2022.
- [9] D. Owerko, F. Gama, and A. Ribeiro, "Optimal power flow using graph neural networks," in *ICASSP 2020-2020 IEEE International Conference on Acoustics, Speech and Signal Processing (ICASSP)*. IEEE, 2020, pp. 5930–5934.
- [10] T. B. Lopez-Garcia and J. A. Domínguez-Navarro, "Optimal power flow with physics-informed typed graph neural networks," *IEEE Transactions on Power Systems*, 2024.
- [11] F. Feng, P. Zhang, M. A. Bragin, and Y. Zhou, "Novel resolution of unit commitment problems through quantum surrogate lagrangian relaxation," *IEEE Transactions on Power Systems*, vol. 38, no. 3, pp. 2460–2471, 2022.
- [12] N. Nikmehr and P. Zhang, "Quantum-inspired power system reliability assessment," *IEEE Transactions on Power Systems*, vol. 38, no. 4, pp. 3476–3490, 2022.
- [13] H. Zhao, P. Zhang, and T.-C. Wei, "A universal variational quantum eigensolver for non-hermitian systems," *Scientific Reports*, vol. 13, no. 1, p. 22313, 2023.
- [14] Z. Kaseb, M. Möller, P. P. Vergara, and P. Palensky, "Power flow analysis using quantum and digital annealers: a discrete combinatorial optimization approach," *Scientific Reports*, vol. 14, no. 1, p. 23216, 2024.
- [15] D. Amaro, M. Rosenkranz, N. Fitzpatrick, K. Hirano, and M. Fiorentini, "A case study of variational quantum algorithms for a job shop scheduling problem," *EPJ Quantum Technology*, vol. 9, no. 1, p. 5, 2022.
- [16] C. Dalyac, L. Henriette, E. Jeandel, W. Lechner, S. Perdrix, M. Porcheron, and M. Veshchezerova, "Qualifying quantum approaches for hard industrial optimization problems. a case study in the field of smart-charging of electric vehicles," *EPJ Quantum Technology*, vol. 8, no. 1, p. 12, 2021.
- [17] T. Morstyn and X. Wang, "Opportunities for quantum computing within net-zero power system optimization," *Joule*, 2024.
- [18] T. Kato, "On the adiabatic theorem of quantum mechanics," *Journal of the Physical Society of Japan*, vol. 5, no. 6, pp. 435–439, 1950.
- [19] T. Albash and D. A. Lidar, "Adiabatic quantum computation," *Reviews of Modern Physics*, vol. 90, no. 1, p. 015002, 2018.
- [20] D. E. Deutsch, "Quantum computational networks," *Proceedings of the royal society of London. A. mathematical and physical sciences*, vol. 425, no. 1868, pp. 73–90, 1989.
- [21] R. Eskandarpour, K. Ghosh, A. Khodaei, L. Zhang, A. Paaso, and S. Bahramirad, "Quantum computing solution of dc power flow," *arXiv preprint arXiv:2010.02442*, 2020.
- [22] B. Sævarsson, S. Chatzivasileiadis, H. Jóhannsson, and J. Østergaard, "Quantum computing for power flow algorithms: Testing on real quantum computers," *arXiv preprint arXiv:2204.14028*, 2022.
- [23] Y. Zhou and P. Zhang, "Noise-resilient quantum machine learning for stability assessment of power systems," *IEEE Transactions on Power Systems*, vol. 38, no. 1, pp. 475–487, 2022.
- [24] Z. Kaseb, M. Möller, G. T. Balducci, P. Palensky, and P. P. Vergara, "Quantum neural networks for power flow analysis," *Electric Power Systems Research*, vol. 235, p. 110677, 2024.
- [25] M. Cerezo, A. Arrasmith, R. Babbush, S. C. Benjamin, S. Endo, K. Fujii, J. R. McClean, K. Mitarai, X. Yuan, L. Cincio *et al.*, "Variational quantum algorithms," *Nature Reviews Physics*, vol. 3, no. 9, pp. 625–644, 2021.
- [26] A. Sagingalieva, M. Kordzanganeh, A. Kurkin, A. Melnikov, D. Kholmistrov, M. Perelshtein, A. Melnikov, A. Skolik, and D. V. Dollen, "Hybrid quantum resnet for car classification and its hyperparameter optimization," *Quantum Machine Intelligence*, vol. 5, no. 2, p. 38, 2023.
- [27] A. Abbas, D. Sutter, C. Zoufal, A. Lucchi, A. Figalli, and S. Woerner, "The power of quantum neural networks," *Nature Computational Science*, vol. 1, no. 6, pp. 403–409, 2021.
- [28] K. Beer, D. Bondarenko, T. Farrelly, T. J. Osborne, R. Salzmann, D. Scheiermann, and R. Wolf, "Training deep quantum neural networks," *Nature communications*, vol. 11, no. 1, p. 808, 2020.
- [29] S. Lloyd, M. Mohseni, and P. Rebentrost, "Quantum algorithms for supervised and unsupervised machine learning," *arXiv preprint arXiv:1307.0411*, 2013.
- [30] T. Morstyn, "Annealing-based quantum computing for combinatorial optimal power flow," *IEEE Transactions on Smart Grid*, vol. 14, no. 2, pp. 1093–1102, 2022.
- [31] A. Narayanan and T. Menneer, "Quantum artificial neural network architectures and components," *Information Sciences*, vol. 128, no. 3–4, pp. 231–255, 2000.
- [32] N. Killoran, T. R. Bromley, J. M. Arrazola, M. Schuld, N. Quesada, and S. Lloyd, "Continuous-variable quantum neural networks," *Physical Review Research*, vol. 1, no. 3, p. 033063, 2019.
- [33] K. He, X. Zhang, S. Ren, and J. Sun, "Deep residual learning for image recognition," in *Proceedings of the IEEE conference on computer vision and pattern recognition*, 2016, pp. 770–778.
- [34] L. Li, Y. Fang, J. Wu, J. Wang, and Y. Ge, "Encoder-decoder full residual deep networks for robust regression and spatiotemporal estimation," *IEEE transactions on neural networks and learning systems*, vol. 32, no. 9, pp. 4217–4230, 2020.
- [35] M. Raissi, P. Perdikaris, and G. E. Karniadakis, "Physics-informed neural networks: A deep learning framework for solving forward and inverse problems involving nonlinear partial differential equations," *Journal of Computational physics*, vol. 378, pp. 686–707, 2019.
- [36] R. Polikar, "Ensemble learning," *Ensemble machine learning: Methods and applications*, pp. 1–34, 2012.
- [37] S. S. Khonde, S. Dhamse, and A. Thosar, "Power quality enhancement of standard IEEE 14 bus system using unified power flow controller," *Int J Eng Sci Innov Technol*, vol. 3, no. 5, 2014.
- [38] M. D. McKay, R. J. Beckman, and W. J. Conover, "A comparison of three methods for selecting values of input variables in the analysis of output from a computer code," *Technometrics*, vol. 42, no. 1, pp. 55–61, 2000.
- [39] A. Paszke, S. Gross, F. Massa, A. Lerer, J. Bradbury, G. Chanan, T. Killeen, Z. Lin, N. Gimelshein, L. Antiga *et al.*, "Pytorch: An imperative style, high-performance deep learning library," *Advances in neural information processing systems*, vol. 32, 2019.
- [40] A. Javadi-Abhari, M. Treinish, K. Krsulich, C. J. Wood, J. Lishman, J. Gacon, S. Martiel, P. D. Nation, L. S. Bishop, A. W. Cross, B. R. Johnson, and J. M. Gambetta, "Quantum computing with Qiskit," 2024.